Proc. Natl. Acad. Sci. USA
Vol. 93, pp. 5363–5367, May 1996
Biochemistry

Insights into antibody catalysis: Structure of an oxygenation catalyst at 1.9-Å resolution

(crystal structure/catalytic antibody/oxidation)

LINDA C. HSIEH-WILSON*†, PETER G. SCHULTZ*†§, AND RAYMOND C. STEVENS†§

*Howard Hughes Medical Institute and †Department of Chemistry, University of California, Berkeley, CA 94720

Contributed by Peter G. Schultz, January 24, 1996

ABSTRACT **The x-ray crystal structures of the sulfide oxidase antibody 28B4 and of antibody 28B4 complexed with hapten have been solved at 2.2-Å and 1.9-Å resolution, respectively. To our knowledge, these structures are the highest resolution catalytic antibody structures to date and provide insight into the molecular mechanism of this antibody-catalyzed monooxygenation reaction. Specifically, the data suggest that entropic restriction plays a fundamental role in catalysis through the precise alignment of the thioether substrate and oxidant. The antibody active site also stabilizes developing charge on both sulfur and periodate in the transition state via cation-pi and electrostatic interactions, respectively. In addition to demonstrating that the active site of antibody 28B4 does indeed reflect the mechanistic information programmed in the aminophosphonic acid hapten, these high-resolution structures provide a basis for enhancing turnover rates through mutagenesis and improved hapten design.**

Antibodies have been shown to catalyze a wide variety of reactions with exquisite control over the reaction pathway (1). However, the further improvement of antibody catalysis depends on high-resolution structural data. The few reported crystal structures of catalytic antibodies have focused, with one exception, on esterolytic reactions (2–6). We now report the three-dimensional structure of an antibody (28B4) that catalyzes the monooxygenation of thioethers. An examination of the structural data may provide insight into enhancing the catalytic efficiencies of antibodies as well as elucidate the mechanisms and evolution of enzymatic catalysis.

Antibody 28B4 catalyzes the periodate-dependent oxidation (Fig. 1) of sulfide **1** to the corresponding sulfoxide **2** (7). Similar oxygen transfer reactions are performed by naturally occurring monooxygenase enzymes for the biosynthesis of steroids and neurotransmitters, the degradation of endogenous substances, and the detoxification of xenobiotics (8, 9). This reaction was initially examined to extend antibody catalysis to this important class of redox reactions and (*ii*) to expand the range of "cofactors" used in biological catalysis. The combination of highly abundant and versatile chemical reagents such as metal hydrides and Lewis acids together with antibody catalysis might lead to a number of advantages over natural enzymes, such as eliminating the need for expensive cofactor recycling in large-scale enzymatic synthesis (10).

The periodate-dependent oxygenation of thioethers can occur either via sulfur attack on the periodate oxygen in a concerted, S_N2-like transition state ($TS^{\ddagger}$) or by initial addition to the iodine center followed by oxygen transfer (Fig. 1). Hammett σ-ρ values, solvent isotope effects, and pH-dependence studies (11, 12) support the former mechanism but do not exclude initial attack on iodine. Antibody 28B4 was raised against aminophosphonic acid hapten **3**, which to a large degree mimics the stereoelectronic features of both transition states. Specifically, hapten **3** contains phosphonate and nitrophenyl moieties designed to provide two binding sites precisely oriented for the periodate and nitroaryl sulfide substrates. Moreover, the positively charged ammonium ion and dianionic phosphonate group mimic the developing charges on sulfur and the periodate oxygens, respectively, in the proposed transition states.

Eight antibodies were found to catalyze the oxidation of substrate **1** and related sulfides with a range of turnover numbers and stereoselectivities. Antibody 28B4, which was among the most efficient, binds hapten **3** with high affinity (K_d= 52 nM) and catalyzes the periodate-dependent oxidation of sulfide **1** with a k_{cat} value of 8.2 s^{-1} (k_{cat}/K_m= 1.9 × 10^5 $M^{-1}\cdot s^{-1}$), similar to the flavin-dependent enzymes (7). To determine the catalytic mechanism of 28B4 and the extent to which the active site evolved in response to mechanistic instructions from the hapten, the free and hapten-bound structures of the antigen-binding fragment (Fab) of the murine antibody 28B4 have been solved to 2.2-Å and 1.9-Å resolution, respectively.

MATERIALS AND METHODS

Fab Preparation and Purification. Monoclonal antibody 28B4 was generated using standard protocols from BALB/c mice immunized with hapten **3** conjugated to the carrier protein keyhole-limpet hemocyanin. Large amounts of full-length antibody were produced in ascites fluid and purified by protein A affinity (Schleicher & Schuell Affinica) chromatography. Fab was prepared using immobilized papain (Pierce) and purified by size exclusion (Sephacryl S-200; Pharmacia) and cation exchange (Mono-S column; Pharmacia) chromatography.

Crystallization. Initial crystallization conditions were obtained using the incomplete crystallization screen of Jancarik and Kim (13). Crystals were grown at 4°C using the hanging-drop procedure in wells containing 0.5 ml of 20% PEG 4K, 10% isopropanol, and 0.1 M Tris (pH 8.5). Drops consisting of a 2-μl aliquot of a protein solution with or without hapten (2 mM hapten and 12.5 mg Fab per ml in 10 mM Tris/100 mM NaCl/1 mM methionine/0.5 mM EDTA, pH 8.5) were mixed with 2 μl of the well solution. Plate-shaped crystals (up to 0.2 × 0.4 × 1.0 mm) belonged to space group P1 with unit-cell dimensions a = 52.7 Å, b = 58.2 Å, c = 43.2 Å, α = 94.3°, β = 113.8°, and γ = 78.9° (Fab-hapten) and a = 47.2 Å, b = 58.6 Å, c = 43.4 Å, α = 95.3°, β = 103.2, and γ = 93.6° (free Fab).

The publication costs of this article were defrayed in part by page charge payment. This article must therefore be hereby marked "*advertisement*" in accordance with 18 U.S.C. §1734 solely to indicate this fact.

Data deposition: The atomic coordinates and structure factors have been deposited in the Protein Data Bank, Chemistry Department, Brookhaven National Laboratory, Upton, NY 11973 [references IKEL (hapten-Fab), IKEM (apo-Fab), R1KELSF (hapten-Fab), and R1KEMSF (apo-Fab)].

§To whom reprint requests should be addressed.

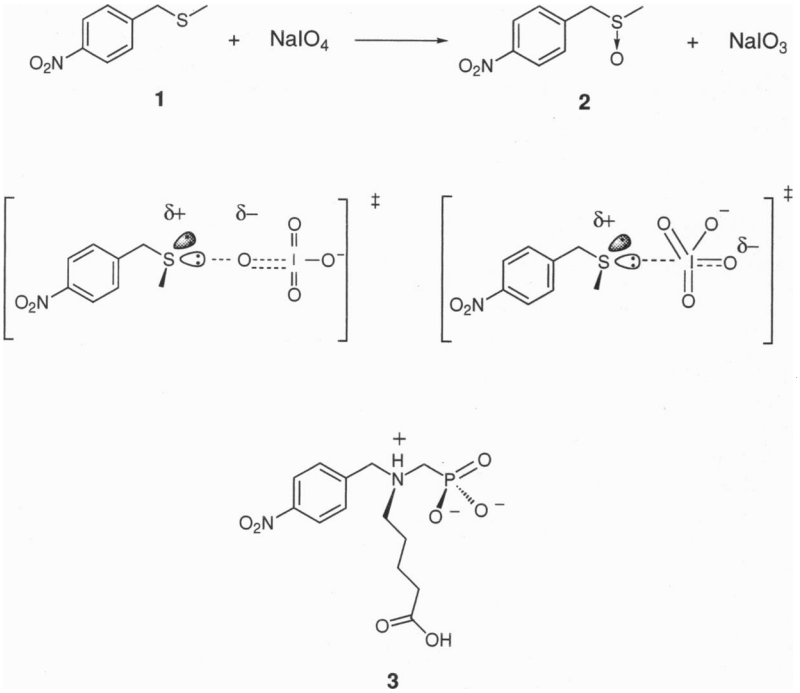

FIG. 1. The periodate ($NaIO_4$)-dependent oxygenation of sulfide **1** can occur via two possible transition states to give sulfoxide product **2**. Hapten **3** mimics the stereoelectronic features of both transition states and was used to raise antibody 28B4.

Data Collection. Data sets were collected at −165°C (Fab-hapten) and 4°C (free Fab) using an R-AXIS II detector system mounted on a Rigaku RU-200 x-ray generator (50 kV and 100 mA). The reflections were indexed using DENZO 1.3.0 (written by Z. Otwinowski) and merged/scaled using the programs ROTAVATA, AGROVATA, and TRUNCATE of the CCP4 suite (14). For the Fab-hapten cocrystals, a total of 83,241 observations were recorded for 31,750 unique reflections. The reduced data set was 98% complete between 20 and 1.9 Å (63% between 1.9 and 1.7 Å) with an R_{merge} value of 0.058. The data set for the uncomplexed Fab, which consisted of 51,820 observations and 21,852 unique reflections, was 98% complete between 20 and 2.2 Å (43% between 2.2 and 2.0 Å) with an R_{merge} value of 0.078.

Structure Determination. The Fab–hapten structure was solved by molecular replacement using the program package AMORE (15) and data in the 15- to 3.0-Å resolution range. Coordinates from the 1igf Fab constant domains (C_L + C_H1) (16) and the AbM-minimized (17) antibody 28B4 variable domains with deletions in the solvent-exposed loop regions were used separately as models for the corresponding parts of the complex. The height of the peak corresponding to the solution was 5 times that of the next highest peak, and the resultant model gave an R factor of 0.48. Alternate rounds of model building with the molecular graphics program O (18) and refinement of the atomic coordinates using X-PLOR version 3.1 (19) were performed until the solvent-exposed loops were rebuilt and the minimization was complete. The final model has an R factor of 19.9% (R_{free} = 25.8) in the 6- to 1.9-Å resolution range. The averaged rms deviations are 0.012 Å and 1.727 Å for the bond lengths and angles, respectively.

The free Fab structure was solved similarly using the hapten-Fab 28B4 structure as the search model. After model building and refinement, the final R factor for the free Fab structure is 18.3% (R_{free} = 28.8) in the 6- to 2.2-Å resolution range, with rms deviations of 0.012 Å and 1.769° Å for the bond lengths and angles, respectively. The stereochemistries of the models were verified with PROCHECK version 2.1.4 (20). The final Fab and Fab-hapten complex structures contain 157 and 306 waters, respectively, and 435 amino acids. The amino acid sequence of the 28B4 Fab has been reported elsewhere (21) with the exception of the N-termini (DVL for the murine light chain and EVKLV for the murine heavy chain). Fab residue numbering follows Kabat numbering (22) throughout.

RESULTS AND DISCUSSION

The hapten is bound in a cleft ≈10 Å deep and 7 Å wide with the aromatic nitro group at the bottom and the phosphonic acid, aliphatic linker, and carboxylic acid groups near the surface of the cleft (Fig. 2). Approximately 212 Å^2 of the hapten (68% of the total solvent-accessible surface) is buried within the Fab. There are 11 van der Waals interactions and

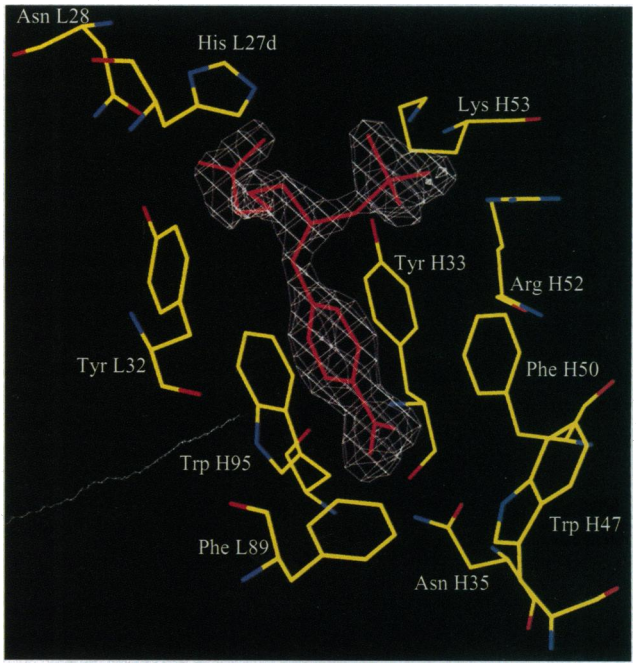

FIG. 2. An F_o-F_c omit electron density map (contoured at 3.5 σ) showing the hapten (red) in the antibody active site. The antibody contacts the hapten (within 3.5 Å) primarily through the CDR loops H1 (H33 and H35), H2 (H50, H52, and H53), H3 (H95), L1 (L32), and L3 (L89).

four hydrogen bonds between the hapten and the antibody, with the majority of the hydrogen bonds and salt bridges (Tyr^{H33}, Arg^{H52}, and Lys^{H53}) contacting the three oxygens of the tetrahedral phosphonate group (Fig. 3). Specifically, the hydroxyl group of Tyr^{H33} (2.5 Å away), the guanidino group of Arg^{H52} (2.8 Å away), and possibly the amino group of Lys^{H53} interact with each of the three oxygens in the tetrahedral phosphonate group. The close proximity of the positively charged guanidinium group of Arg^{H52} and the ε-amino group of Lys^{H53} should also produce large, favorable electrostatic interactions with the dianionic phosphonate group. Interestingly, recognition of the phosphonate moiety by 28B4 is very similar to recognition of the phosphocholine phosphate group by the McPC603 antibody (23). In fact, the two antibodies share the same germ-line family of V_H region genes (22 and 24; P. L. Yang, personal communication). That this conserved phosphonate binding site acts as a periodate binding pocket is consistent with kinetic analysis of 28B4, which shows a Michaelis constant (K_m) of 252 μM for sodium periodate (7).

The structure also confirms earlier observations demonstrating the specificity of antibody 28B4 for *p*-nitroaryl substrates (7). (Antibody 28B4 does not catalyze oxygenation of benzyl methyl sulfide.) The nitrophenyl ring of hapten **3** is deeply embedded in a hydrophobic cavity (Trp^{H95}, Tyr^{H33}, Trp^{H47}, Phe^{L89}, and Phe^{H50}) and sandwiched between the aromatic rings of Trp^{H95} and Phe^{H50} (≈3.5 Å away from the hapten; Fig. 3). Specific recognition of the *p*-nitro group is achieved through Asn^{H35}, which is asymmetrically hydrogen-bonded between the two oxygens of the buried nitro group (2.9 Å and 3.5 Å away from ND2). Asn^{H35} may be the sole determinant of the selectivity for nitro-containing substrates. Preliminary analysis of the Kabat database suggests that Asn^{H35} corresponds to a somatic mutation in the affinity maturation of 28B4 from the V11 germ-line gene (22; P. L. Yang, personal communication). Good complementarity is observed for the positively charged ammonium moiety, which mimics the developing charge on sulfur in the TS‡. A favorable interaction occurs between the ammonium ion and the aromatic π-system of Tyr^{L32} (3.9 Å from the benzylic carbon); such "amino–aromatic" interactions have been previously observed in McPC603 and other protein structures (25, 26).

The highly selective contacts to the nitroaryl moiety contrast with the relatively nonspecific recognition of the aliphatic linker functionality of hapten **3**. The solvent accessibility of the

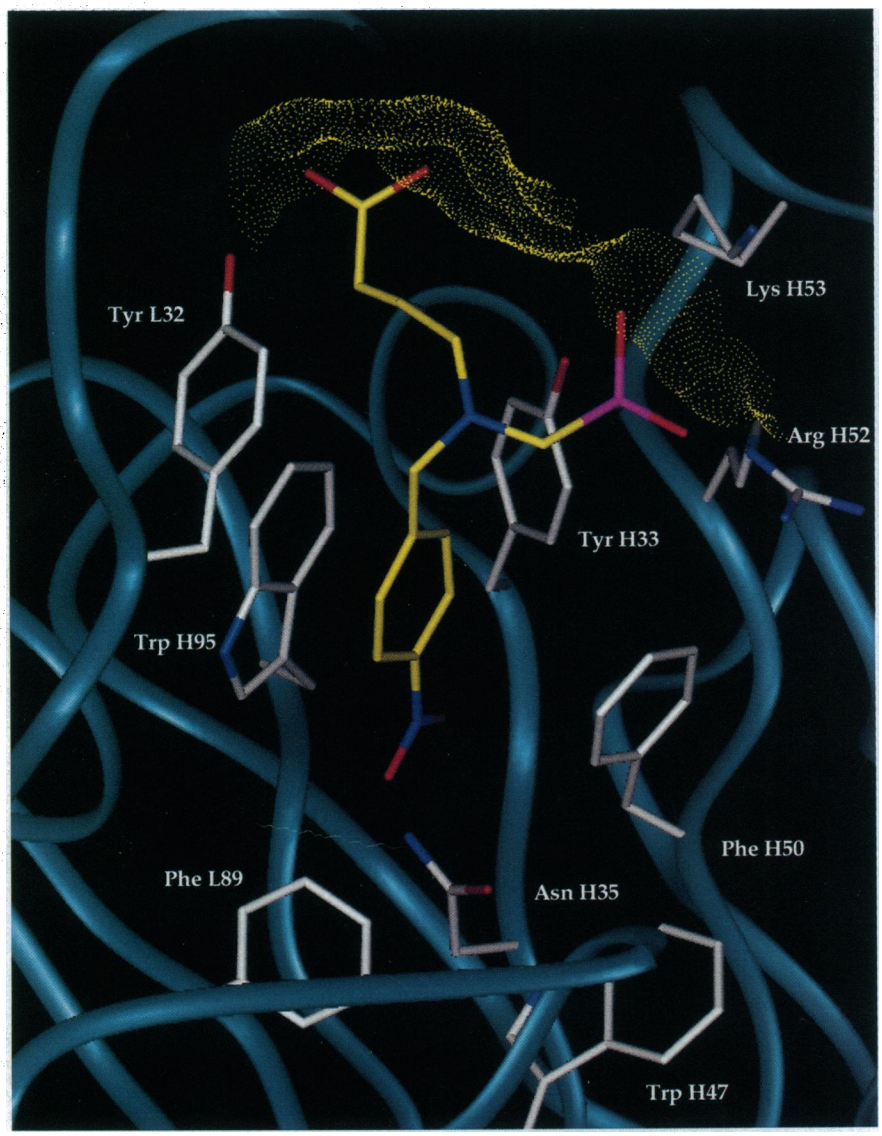

FIG. 3. Structure of the 28B4 active site showing the aminophosphonic acid hapten (yellow) and its solvent-accessible surface (yellow dots). The aromatic nitro group is buried in a hydrophobic pocket, and the aliphatic linker and phosphonate moieties reside near the surface. The solvent accessiblity of the linker may reflect the influence of the carrier protein upon hapten presentation. The Cα backbone is shown in blue and the side chains of important residues in white (heteroatom colors: O, red; N, blue; and P, pink).

linker may reflect the influence of the carrier protein upon hapten presentation. Studies probing the substrate specificity of 28B4 are consistent with these observations and demonstrate that the aliphatic substituent, in contrast to the nitroaryl ring, can be replaced with a variety of other functional groups (7). Indeed, the limited antibody complementarity to this region may be responsible for the modest enantioselectivity of 28B4 (16% enantiomeric excess for chiral sulfoxide formation). These results reinforce the intuitive notion that more rigid or immunogenic elements in the linker may improve antibody–hapten complementarity, thus affording a more enantioselective catalyst.

The overall data suggests that both entropic and enthalpic factors contribute to catalysis. A network of hydrogen bonding, electrostatic, and π-stacking interactions lock the periodate ion and nitroaryl substrate into a reactive orientation. Thus, a large component of the antibody binding energy may function as an "entropy trap" to freeze out rotational and translational degrees of freedom in the TS‡ (27). In addition to aligning the periodate cofactor, residues Tyr^{H33}, Arg^{H52}, and Lys^{H53} may stabilize the developing negative charge on the periodate oxygens in the TS‡. The developing positive charge on sulfur in the TS‡ may be stabilized by the electron-rich aromatic ring of Tyr^{L32} via a putative cation-pi interaction. Such interactions have been invoked to explain cyclophane-catalyzed S_N2 reactions, acetylcholine recognition, and the ion selectivity of channel proteins (26, 28, 29). The close van der Waals contact between Tyr^{L32} and the benzylic carbon of the hapten may also explain the high rate of acceleration for *p*-nitrothioanisole oxidation (7). The nonoverlapping binding sites for the periodate and thioether substrates, one at the surface and the other buried, are consistent with the random-binding, sequential kinetic mechanism observed (7).

In addition to identifying active site residues important for catalysis, this study provides the first opportunity to compare the bound and unbound forms of a catalytic antibody directly. Such comparisons offer a glimpse into the mechanism of antibody–substrate association and directly address the issue of antibody-combining site flexibility (30–32). In this example, small side chain and main chain rearrangements consistent with the lock-and-key mechanism (33) occur upon hapten binding (Fig. 4; rms main chain deviation for variable domains, 0.31 Å). Notably, Tyr^{H33} moves ≈0.6 Å closer to the haptenic phosphonate oxygens, and the indole ring of Trp^{H95} stacks (≈0.5 Å) more closely with the nitroaryl ring. Moreover, the side chain of Lys^{H53}, which has ill-defined electron density in the unbound form, appears to be oriented toward the phosphonate moiety in the hapten-bound form. With the exception of Tyr^{L32}, which undergoes a small main chain movement toward the hapten (rms deviation, 0.45 Å), the CDR loop L1 (primarily L28-35; rms deviation, 0.44–0.98 Å) moves away from the hapten, presumably to accommodate it. Molecular dynamics simulations confirm the flexibility of the Tyr^{L32} side chain, which makes very few electrostatic and van der Waals contacts with the rest of the protein. Dynamic conformational changes of this sort are likely to play an important role in the

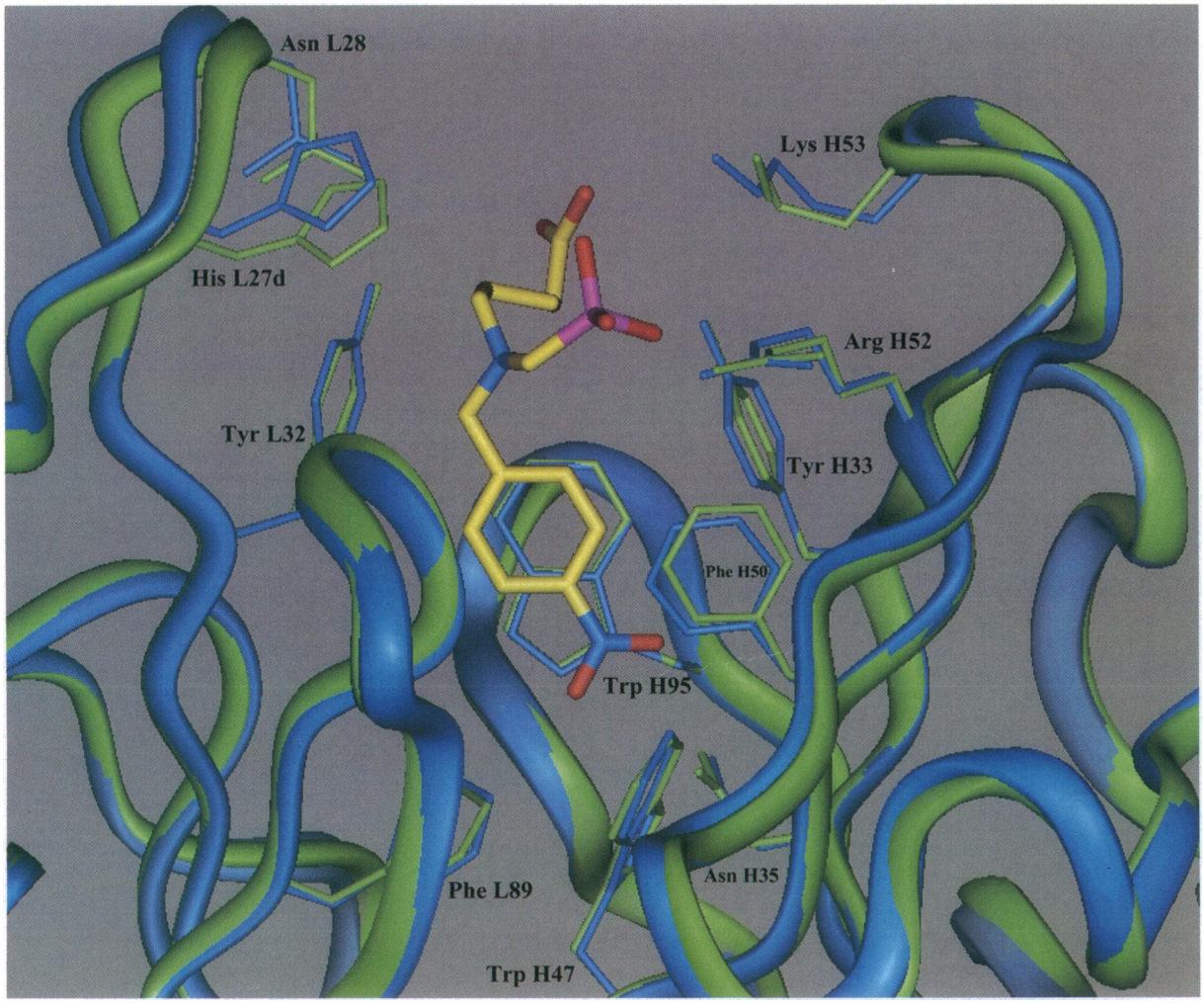

FIG. 4. Superposition of the hapten-Fab and free Fab structures. The hapten-bound structure is depicted in blue and the apo-Fab structure in green.

reorganization of antibody active sites into the Michaelis complex and the optimum geometry for $TS^{\ddagger}$ stabilization.

The structure of the antibody–hapten complex identifies specific mutations that may clarify the catalytic mechanism of antibody 28B4 and improve its efficiency and stereoselectivity. For example, mutation of Tyr^{L32} to a phenylalanine or tryptophan should provide insight into the importance of the putative cation-pi interaction. Furthermore, the introduction of negatively charged residues proximal to the haptenic ammonium group (for example, Ser^{L92} or Asn^{L28} to Glu) and additional hydrogen bonds to the phosphonate moiety (Phe^{H50} to Tyr) may enhance the catalytic activity of 28B4. It may be possible to improve the enantioselectivity of 28B4 by optimizing the antibody–hapten shape complementarity around the linker moiety (His^{L27d} to Trp; Asn^{L28} to Gln). In addition to mutagenesis studies, new hapten designs replacing the aliphatic linker with more rigid or immunogenic functionalities to restrict the mobility of the sulfur moiety may enhance the stereoselectivity and efficiency of the elicited antibodies. Hapten designs that improve ammonium ion recognition (linkage to carrier protein via the aryl ring) or modulate the relative positions of the thioether and periodate substrates (replacement of the phosphonate moiety with an arsonate or sulfonate group) may also increase turnover rates. Finally, sequence and structural comparisons to other existing antibodies raised against hapten **3** with varying sulfide oxidase activity and stereoselectivity should dramatically increase our understanding of the relationship between combining site geometry and catalytic efficiency.

We gratefully acknowledge R. Crawford and O. Littlefield for assistance with the data collection. We thank H. Ulrich, G. Wedemayer, T. Wilson, and P. Yang for helpful discussions. This work was supported by the National Institutes of Health (Grant No. RO1AI24695). P.G.S. is a Howard Hughes Medical Institute Investigator. L.C.H.-W. thanks the National Science Foundation and American Chemical Society for predoctoral fellowships.

1. Schultz, P. G. & Lerner, R. A. (1995) *Science* **269,** 1835–1842.
2. Zhou, G. W., Guo, J., Huang, W., Fletterick, R. J. & Scanlan, T. S. (1994) *Science* **265,** 1059–1064.
3. Haynes, M. R., Stura, E. A., Hilvert, D. & Wilson, I. A. (1994) *Science* **263,** 646–652.
4. Charbonnier, J.-B., Carpenter, E., Gigant, B., Golinelli-Pimpaneau, B., Eshhar, Z., Green, B. S. & Knossow, M. (1995) *Proc. Natl. Acad. Sci. USA* **92,** 11721–11725.
5. Golinelli-Pimpaneau, B., Gigant, B., Bizebard, T., Navaza, J., Saludjian, P., Zemel, R., Tawfik, D. S., Eshhar, Z., Green, B. S. & Knossow, M. (1994) *Structure* **2,** 175–183.
6. Patten, P. A., Gray, N. S., Yang, P. L., Marks, C. B., Wedemayer, G. J., Boniface, J. J., Stevens, R. C. & Schultz, P. G. (1996) *Science* **271,** 1086–1091.
7. Hsieh, L. C., Stephans, J. C. & Schultz, P. G. (1994) *J. Am. Chem. Soc.* **116,** 2167–2168.
8. Walsh, C. & Latham, J. (1986) *J. Protein Chem.* **5,** 79–87.
9. Jakoby, W. B. & Ziegler, D. M. (1990) *J. Biol. Chem.* **265,** 20715–20718.
10. Wong, C.-H. (1989) *Science* **244,** 1145–1152.
11. Ruff, F. & Kucsman, A. (1985) *J. Chem. Soc. Perkin Trans.* **2,** 683–686.
12. Ruff, F. & Kucsman, A. (1988) *J. Chem. Soc. Perkin Trans.* **2,** 1123–1128.
13. Jancarik, J. & Kim, S. H. (1991) *J. Appl. Crystallogr.* **24,** 409–411.
14. Daresbury Laboratory (1979) *CCP4-The SERC (UK) Collaborative Computing Project No. 4, A Suite of Programs for Protein Crystallography* (Daresbury Lab., Warrington, UK).
15. Navaza, J. (1994) *Acta Crystallogr. A* **50,** 157–163.
16. Stanfield, R. L., Fieser, T. M., Lerner, R. A. & Wilson, I. A. (1990) *Science* **248,** 712–719.
17. Oxford Molecular (1994) *AbM User Guide* (Oxford Molecular Limited, Oxford, United Kingdom), Issue 4.
18. Jones, T. A. & Kjeldgaard, M. (1993) O *(Uppsala Univ., Uppsala, Sweden).*
19. Brünger, A. T. (1992) X-PLOR *Version 3.1: A System for Crystallography and NMR* (Yale Univ. Press, New Haven, CT).
20. Laskowski, R. A., MacArthur, M. W., Moss, D. S. & Thornton, J. M. (1993) *J. Appl. Crystallogr.* **26,** 283–291.
21. Ulrich, H. D., Patten, P. A., Yang, P. L., Romesberg, F. E. & Schultz, P. G. (1995) *Proc. Natl. Acad. Sci. USA* **92,** 11907–11911.
22. Kabat, E. A., Wu, T. T., Perry, H. M., Gottesman, K. S. & Foeller, C. (1991) *Sequences of Proteins of Immunological Interest* (U.S. Department of Health and Human Services, Bethesda, MD), NIH Pub. 91–3242.
23. Segal, D. M., Padlan, E. A., Cohen, G. H., Rudikoff, S., Potter, M. & Davies, D. R. (1974) *Proc. Natl. Acad. Sci. USA* **71,** 4298–4302.
24. Crews, S., Griffin, J., Huang, H., Calame, K. & Hood, L. (1981) *Cell* **25,** 59–66.
25. Burley, S. K. & Petsko, G. A. (1985) *Science* **229,** 23–28.
26. Dougherty, D. A. & Stauffer, D. A. (1990) *Science* **250,** 1558–1560.
27. Page, M. I. & Jencks, W. P. (1971) *Proc. Natl. Acad. Sci. USA* **68,** 1678–1683.
28. McCurdy, A., Jimenez, L., Stauffer, D. A. & Dougherty, D. A. (1992) *J. Am. Chem. Soc.* **114,** 10314–10321.
29. Kumpf, R. A. & Dougherty, D. A. (1993) *Science* **261,** 1708–1710.
30. Arevalo, J. H., Taussig, M. J. & Wilson, I. A. (1993) *Nature (London)* **365,** 859–863.
31. Davies, D. R., Padlan, E. A. & Sheriff, S. (1990) *Annu. Rev. Biochem.* **59,** 439–473.
32. Wilson, I. A. & Stanfield, R. L. (1994) *Curr. Opin. Struct. Biol.* **4,** 857–867.
33. Amit, A. G., Mariuzza, R. A., Phillips, S. E. V. & Poljak, R. J. (1986) *Science* **233,** 747–753.